

International Journal of Modern Physics C  
 © World Scientific Publishing Company

## Lattice Boltzmann Approach to High-Speed Compressible Flows

X. F. Pan, Aiguo Xu\* Guangcai Zhang, Song Jiang

*National Key Laboratory of Computational Physics, Institute of Applied Physics and  
 Computational Mathematics, P.O.Box 8009-26, Beijing 100088, P.R.China  
 E-mail: Xu\_Aiguo@iapcm.ac.cn*

Received 23 April 2007  
 Revised 4 June 2007

We present an improved lattice Boltzmann model for high-speed compressible flows. The model is composed of a discrete-velocity model by Kataoka and Tsutahara [Phys. Rev. E **69**, 056702 (2004)] and an appropriate finite-difference scheme combined with an additional dissipation term. With the dissipation term parameters in the model can be flexibly chosen so that the von Neumann stability condition is satisfied. The influence of the various model parameters on the numerical stability is analyzed and some reference values of parameter are suggested. The new scheme works for both subsonic and supersonic flows with a Mach number up to 30 (or higher), which is validated by well-known benchmark tests. Simulations on Riemann problems with very high ratios (1000 : 1) of pressure and density also show good accuracy and stability. Successful recovering of regular and double Mach shock reflections shows the potential application of the lattice Boltzmann model to fluid systems where non-equilibrium processes are intrinsic. The new scheme for stability can be easily extended to other lattice Boltzmann models.

*Keywords:* Lattice Boltzmann; high-speed compressible flow; von Neumann Analysis; shock.

### 1. Introduction

High-speed compressible flow with shocks plays an important role in various fields, such as explosion physics, aeronautics, etc. Efficient simulation of such a system is interesting and challenging. The traditional method is based on a set of macroscopic Euler equations resolved by the Finite-element or Finite-volume schemes, where the artificial viscosity is applied or the Riemann solver is used to capture the shock<sup>1,2,3</sup>. According to the gas kinetic theory, a set of Euler equations describes a system being at equilibrium. For a system with shocks, the non-equilibrium behavior is intrinsic, so a scheme based on the fundamental kinetic theory is to be preferred. As a new approach to fluid dynamics, the lattice Boltzmann (LB) method<sup>4</sup> solves the fully discrete Boltzmann equation by using an appropriate difference scheme to the temporal and spatial derivatives of the distribution function  $f_i(\mathbf{x}, t)$ , where  $\mathbf{x}$

\*Corresponding author

2 *Pan, Xu, Zhang, Jiang*

and  $t$  are the position and time, respectively, and the index  $i$  corresponds to the  $i$ -th discrete velocity. It recovers the desired macroscopic equations in the hydrodynamic limit and has the potential to fill the gap between continuum description and molecular dynamics<sup>5</sup>. Besides the traditional LB originating from the lattice gas cellular automata<sup>6,7,8,9,10</sup>, other versions such as finite-difference(FD)<sup>11,12,13,14,15</sup>, finite-volume(FV)<sup>16</sup>, and finite-element(FE)<sup>17</sup>, etc have also been developed under the same framework. Among these works, developing LB models for high-speed compressible flows has long been attempted by different authors<sup>15,18</sup>. Among the existing models for two-dimensional compressible fluids, the one by Kataoka and Tsutahara(KT)<sup>15</sup> has a simple and rigorous theoretical background. It takes flexible ratio of specific-heat and is superior in computational efficiency because the total number of its discrete velocity is reduced to 9. But similar to previous LB models<sup>19</sup>, the numerical stability problem remains one of the few blocks for its practical simulation to high-Mach-number compressible flows. In this paper we present a new scheme based on the original discrete-velocity-model (DVM) by KT and an appropriate finite-difference scheme combined an additional dissipation term. With the new scheme fluid systems with high-Mach-number and/or high ratios of pressure and density can be successfully simulated.

This paper is organized as follows. In section 2 the original discrete-velocity-model by KT is briefly reviewed and an alternative FD scheme is proposed for later analysis and using. A von Neumann stability analysis is performed in section 3, from which solutions to improve the numerical stability can be found. Several benchmark tests are used to validate the proposed scheme in section 4. Section 5 concludes the present paper.

## 2. Description of the DVM and FD scheme

The LB equation with the Bhatnager-Gross-Krook approximation<sup>20</sup> reads,

$$\frac{\partial f_i}{\partial t} + v_{i\alpha} \frac{\partial f_i}{\partial x_\alpha} = \frac{1}{\tau} [f_i^{eq} - f_i], \quad (1)$$

where  $f_i^{eq}$  is the discrete version of the local equilibrium distribution function;  $\tau$  the relaxation time; index  $\alpha = 1, 2, 3$  corresponding to  $x, y$ , and  $z$ , respectively; and  $v_i$  the  $i$ -th discrete velocity,  $i = 0, \dots, N - 1$ ;  $N$  is the total number of the discrete velocity. Under the hydrodynamic limit the LB equation is required to describe the following Euler equations,

$$\begin{aligned} \frac{\partial \rho}{\partial t} + \frac{\partial(\rho u_\alpha)}{\partial x_\alpha} &= 0, \\ \frac{\partial(\rho u_\alpha)}{\partial t} + \frac{\partial(\rho u_\alpha u_\beta)}{\partial x_\beta} + \frac{\partial P}{\partial x_\alpha} &= 0, \\ \frac{\partial \rho(bRT + u_\alpha^2)}{\partial t} + \frac{\partial \rho u_\alpha(bRT + u_\beta^2) + 2P u_\alpha}{\partial x_\beta} &= 0, \end{aligned} \quad (2)$$

where  $\rho$ ,  $u$ ,  $T$ ,  $P$  ( $= \rho RT$ ) are the hydrodynamic density, flow velocity, temperature and pressure, respectively, and  $R$  is the specific gas constant,  $b$  relates to the specific-heat ratio  $\gamma$  as follows,  $b = 2/(\gamma - 1)$ . The following constraints are imposed on the moments of  $f_i^{eq}$  and  $f_i$ ,

$$\rho = \sum_{i=0}^{N-1} f_i^{eq} = \sum_{i=0}^{N-1} f_i, \quad (3)$$

$$\rho u_\alpha = \sum_{i=0}^{N-1} f_i^{eq} v_{i\alpha} = \sum_{i=0}^{N-1} f_i v_{i\alpha}, \quad (4)$$

$$\rho(bRT + u_\alpha^2) = \sum_{i=0}^{N-1} f_i^{eq} (v_{i\alpha}^2 + \eta_i^2) = \sum_{i=0}^{N-1} f_i (v_{i\alpha}^2 + \eta_i^2), \quad (5)$$

$$P\delta_{\alpha\beta} + \rho u_\alpha u_\beta = \sum_{i=0}^{N-1} f_i^{eq} v_{i\alpha} v_{i\beta}, \quad (6)$$

$$\rho[(b+2)RT + u_\beta^2]u_\alpha = \sum_{i=0}^{N-1} f_i^{eq} (v_{i\alpha}^2 + \eta_i^2)v_{i\alpha}, \quad (7)$$

where  $\eta_i$  is another variable introduced to make specific-heat ratio flexible<sup>a</sup>.

Equation (1) may be written in non-dimensional form by using a characteristic flow length scale  $L$ , reference speed  $e_r$  and density  $\rho_r$ . Two reference time scales are used,  $t_c$  to represent the time between particle collisions and  $L/e_r$  to present a characteristic flow time. The resulting non-dimensional equation is

$$\frac{\partial \hat{f}_i}{\partial \hat{t}} + \hat{v}_{i\alpha} \frac{\partial \hat{f}_i}{\partial \hat{x}_\alpha} = \frac{1}{\varepsilon \hat{\tau}} [\hat{f}_i^{eq} - \hat{f}_i], \quad (8)$$

where the caret symbols are used to denote non-dimensional quantities  $\hat{v}_{i\alpha} = v_{i\alpha}/e_r$ ,  $\hat{t} = te_r/L$ ,  $\hat{\tau} = \tau/t_c$ , and  $\hat{f}_i = f_i/\rho_r$ . The parameter  $\varepsilon = t_c e_r/L$  is the Knudsen number which may be interpreted as either the ratio of collision time to flow time or as the ratio of mean free path to the characteristic flow length. We will not use the caret notation further but will assume that the equation are in non-dimensional form henceforth.

In the two-dimensional case, the KT discrete velocity model has nine components. It reads

$$(v_{i1}, v_{i2}) = \begin{cases} (0, 0), i = 0 \\ c_1 \left( \cos\left(\frac{\pi(i+1)}{2}\right), \sin\left(\frac{\pi(i+1)}{2}\right) \right), i = 1, 2, 3, 4 \\ c_2 \left( \cos\pi\left(\frac{i+1}{2} + \frac{1}{4}\right), \cos\pi\left(\frac{i+1}{2} + \frac{1}{4}\right) \right), i = 5, 6, 7, 8 \end{cases} \quad (9)$$

<sup>a</sup>In a practical system, the ratio  $\gamma$  provides information on the internal degrees of freedom of molecules. For example,  $\gamma$  has a certain well-known value for an ideal, monatomic gas (like helium), and is different for diatomic molecules like those that make up most of the atmosphere. To formulate the DVM, the discretization and contribution of the internal degrees of freedoms of the molecules are represented by the constraints (5) and (7).

4 Pan, Xu, Zhang, Jiang

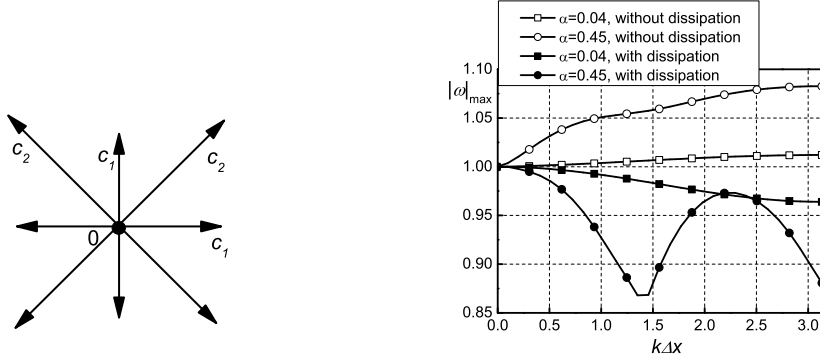


Fig. 1. (Left above) Schematic figure of the discrete velocity model.

 Fig. 2. (Right above) Effects of the dissipation term. Parameters used are  $\rho = 1.0$ ,  $T = 1.0$ ,  $u_1 = 10.0$ ,  $u_2 = 0.0$ , the remaining constants are set as  $c_1 = 10$ ,  $c_2 = 20$ ,  $\eta_0 = 10$ ,  $\Delta t = \alpha \Delta x / c_2$ 

$$\eta_i = \begin{cases} \eta_0 & i = 0 \\ 0 & i = 1, 2, \dots, 8 \end{cases} \quad (10)$$

A schematic figure of the distribution of the discrete velocities is shown in Fig.1, where  $c_1$  and  $c_2$  are constants which should not depart faraway from the flow velocity  $u$  and  $c_2$  is generally chosen 1.0 ~ 3.0 times of  $c_1$ .

The local equilibrium distribution function is computed by

$$f_i^{eq} = \rho(A_i + B_i v_{i\alpha} u_\alpha + D_i u_\alpha v_{i\alpha} u_\beta v_{i\beta}), \quad i = 0, 1, 2, \dots, 8, \quad (11)$$

where

$$A_i = \begin{cases} \frac{b-2}{\eta_0} T, & i = 0 \\ \frac{1}{4(c_1^2 - c_2^2)} \left[ -c_2^2 + \left( (b-2) \frac{c_2^2}{\eta_0^2} + 2 \right) T + \frac{c_2^2}{c_1^2} u_\alpha^2 \right], & i = 1, 2, 3, 4 \\ \frac{1}{4(c_2^2 - c_1^2)} \left[ -c_1^2 + \left( (b-2) \frac{c_1^2}{\eta_0^2} + 2 \right) T + \frac{c_1^2}{c_2^2} u_\alpha^2 \right], & i = 5, 6, 7, 8 \end{cases} \quad (12)$$

$$B_i = \begin{cases} 0, & i = 0 \\ \frac{-c_2^2 + (b+2)T + u_\beta^2}{2c_1^2(c_1^2 - c_2^2)}, & i = 1, 2, 3, 4 \\ \frac{-c_1^2 + (b+2)T + u_\beta^2}{2c_2^2(c_2^2 - c_1^2)}, & i = 5, 6, 7, 8 \end{cases}, \quad D_i = \begin{cases} 0, & i = 0 \\ \frac{1}{2c_1^4}, & i = 1, 2, 3, 4 \\ \frac{1}{2c_2^4}, & i = 5, 6, 7, 8 \end{cases} \quad (13)$$

It is clear that  $\eta_0$ ,  $c_1$  and  $c_2$  are independent parameters in this DVM and the value of  $\eta_0$  influences the discrete local equilibrium distribution function  $f_i^{eq}$  via the expansion coefficient  $A_i$ . The combination of the above DVM and the general FD scheme with first-order forward in time and second-order upwinding in space composes the original FDLB model by KT. The FDLB by KT has been validated via the Riemann problem in subsonic flows<sup>15</sup>. In a LB simulation the discretization in time and space introduces unphysical waves, and the collision term introduces

a physical dissipation when the system deviates from the local equilibrium. If the physical dissipation is strong enough so that the unphysical oscillations are not to be amplified in the simulation procedure, we will have no instability problem. The original LB model by KT is not stable when the Mach number  $M$  exceeds 1<sup>15</sup>, which shows that an additional dissipation term is needed in such cases. To make practical the LB simulation to the supersonic flows, we propose an alternative FD scheme in the following part of this section. The proposed FD scheme will be combined with an additional dissipation term to overcome the numerical instability problem in the next section.

We use the usual first-order forward scheme in time. Since all the quantities are now non-dimensional, to simplify the following analysis, the time step  $\Delta t$  is set to be numerically equal to the Knudsen number  $\varepsilon$ . Thus, from Eq.(8) we have

$$f_i(\mathbf{x}, t + \Delta t) - f_i(\mathbf{x}, t) + v_{i\alpha} \frac{\partial f_i(\mathbf{x}, t)}{\partial x_\alpha} \Delta t = \frac{1}{\tau} [f_i^{eq}(\mathbf{x}, t) - f_i(\mathbf{x}, t)]. \quad (14)$$

In Eq.(14) the spatial derivative  $\partial f_i / \partial x$  can be calculated by

$$\text{If } v_{ix} \geq 0, \quad \frac{\partial f_i}{\partial x} = \frac{\beta f_i(x + \Delta x, t) + (1 - 2\beta) f_i(x, t) - (1 - \beta) f_i(x - \Delta x, t)}{\Delta x}; \quad (15)$$

$$\text{If } v_{ix} < 0, \quad \frac{\partial f_i}{\partial x} = \frac{(1 - \beta) f_i(x + \Delta x, t) - (1 - 2\beta) f_i(x, t) - \beta f_i(x - \Delta x, t)}{\Delta x}. \quad (16)$$

In Eqs.(15) and (16),  $0 \leq \beta \leq 0.5$ . If  $\beta$  takes zero, then they are not other than the first order upwind scheme in space; if  $\beta$  takes 0.5, they recover to the general central difference scheme.  $\partial f_i / \partial y$  can be calculated in a similar way. Actually, Eqs.(15) and (16) can be rewritten as

$$\text{If } v_{ix} \geq 0, \quad \frac{\partial f_i}{\partial x} = \frac{f_i(x, t) - f_i(x - \Delta x, t)}{\Delta x} + \frac{\beta \Delta x [f_i(x + \Delta x, t) + f_i(x - \Delta x, t) - 2f_i(x, t)]}{\Delta x^2}; \quad (17)$$

$$\text{If } v_{ix} < 0, \quad \frac{\partial f_i}{\partial x} = \frac{f_i(x + \Delta x, t) - f_i(x, t)}{\Delta x} - \frac{\beta \Delta x [f_i(x + \Delta x, t) + f_i(x - \Delta x, t) - 2f_i(x, t)]}{\Delta x^2}. \quad (18)$$

The second terms in the right-hand-side of Eqs.(17) and (18) can be regarded as some kind of artificial viscosities which are used to reduce some unphysical phenomena such as wall-heating<sup>22</sup>, but they are not enough to be effectively improve the stability of LB simulation, which means additional dissipation term is needed for a practical LB simulation. In the following sections the parameter  $\beta$  is chosen to be 0.25 if not particularly stated.

6 *Pan, Xu, Zhang, Jiang*

### 3. von Neumann Analysis

The stability problem of LB has been addressed and attempted for some years 4,19,21,23,24,25,26,27 . Among them, the the entropic LB method<sup>23,24</sup> tries to make the scheme to follow the  $H$ -theorem; The FIX-UP method<sup>23,25</sup> is based on the standard BGK scheme, uses a third order equilibrium distribution function and a self-adapting updating parameter to avoid negativeness of the mass distribution function. Flux limiter techniques are used to enhance the stability of FDLB by Sofonea, et al<sup>26</sup>. Adding minimal dissipation locally to improve stability is also suggested by Brownlee, et al<sup>27</sup>, but there such an approach is not explicitly discussed. All the above mentioned attempts are for low Mach number flows. In this paper we focus mainly on high speed flows.

Following Seta, et al<sup>11</sup>, in this paper we resort to the von Neumann stability analysis to compose a stable LB scheme where the additional dissipation is effective and minimal. The following analysis is based on the FD scheme shown in Eqs.(17) and (18). In the von Neumann analysis the solution of finite-difference equation is written as the familiar Fourier series, and the numerical stability is evaluated by the magnitude of eigenvalues of an amplification matrix. The small perturbation  $\Delta f_i$  is defined as  $f_i(\mathbf{x}, t) = \Delta f_i(\mathbf{x}, t) + \bar{f}_i^0$ , where  $\bar{f}_i^0$  is the global equilibrium distribution function and is a constant which does not vary in space or time and depends only on the mean density, velocity and temperature. From Eq. (14) we can obtain

$$\Delta f_i(\mathbf{x}, t + \Delta t) - \Delta f_i(\mathbf{x}, t) + v_{i\alpha} \frac{\partial \Delta f_i}{\partial x_\alpha} \Delta t = \frac{\Delta f_j}{\tau} \left[ \frac{\partial f_i^{eq}}{\partial f_j} - 1 \right]. \quad (19)$$

The perturbation part  $\Delta f_i(\mathbf{x}, t)$  may be written as series of complex exponents,  $\Delta f_i(\mathbf{x}, t) = F_i^t \exp(i\mathbf{k} \cdot \mathbf{x})$ , where  $F_i^t$  is an amplitude at grid point  $\mathbf{x}$  and time  $t$ ,  $i$  is an imaginary unit, and  $k_\alpha$  is the wave number of sine wave in the domain with the highest resolution  $1/\Delta x_\alpha$ . From Eqs. (19) we obtain  $F_i^{t+\Delta t} = G_{i,j} F_j^t$ , where  $G_{ij}$  is a matrix being used to assess amplification rate of  $F_i^t$  per time step  $\Delta t$ . If the maximum of the eigenvalues of the amplification matrix satisfies the condition,  $\max|\omega| \leq 1$ , for all wave numbers, the FD scheme is surely stable, where  $\omega$  is the eigenvalue of the amplification matrix. This is the von Neumann condition for stability.

The amplification matrix  $\mathbf{G}$  can be written as following,

$$G_{ij} = \left( 1 - \frac{v_{i\alpha} \Delta t}{\Delta x_\alpha} \phi - \frac{1}{\tau} \right) \delta_{ij} + \frac{1}{\tau} \frac{\partial f_i^{eq}}{\partial f_j} \quad (20)$$

where

$$\phi = \begin{cases} \beta \exp(ik_\alpha \Delta x_\alpha) + (1 - 2\beta) - (1 - \beta) \exp(-ik_\alpha \Delta x_\alpha), & \text{if } v_{i\alpha} \geq 0; \\ (1 - \beta) \exp(ik_\alpha \Delta x_\alpha) - (1 - 2\beta) - \beta \exp(-ik_\alpha \Delta x_\alpha), & \text{if } v_{i\alpha} < 0. \end{cases} \quad (21)$$

Several researchers have analyzed the stability of the incompressible LB models<sup>11,28,29</sup>, it is found that there is not a single wave-number being always the most unstable. For the 2D DVM by KT  $\mathbf{G}$  is a matrix with  $9 \times 9$  elements.

Every element is related to the macroscopical variables (density, temperature, velocities), discrete velocities and other constants, so it is difficult to analyze with explicit expressions. We resort to the software, Mathematica-5.

In order to simulate high-speed flows, we introduce the following dissipation term to the LB equation,

$$f_i(\mathbf{x}, t+\Delta t) - f_i(\mathbf{x}, t) + v_{i\alpha} \frac{\partial f_i(\mathbf{x}, t)}{\partial x_\alpha} \Delta t - \lambda_i \sum_{\alpha=1}^2 \frac{\partial^2 f_i(\mathbf{x}, t)}{\partial x_\alpha^2} \Delta t = \frac{1}{\tau} [f_i^{eq}(\mathbf{x}, t) - f_i(\mathbf{x}, t)] \quad (22)$$

where  $\lambda_i$  is a small number not varying in space or time. The second-order derivative  $\frac{\partial^2 f_i(\mathbf{x}, t)}{\partial x_\alpha^2}$  can be calculated by the central difference scheme. Then  $G_{i,j}$  can be written as

$$G_{i,j} = \frac{\partial f_i^{eq}}{\partial f_j} - \frac{v_{i\alpha} \Delta t}{\Delta x_\alpha} \phi \delta_{ij} - \lambda_i \sum_{\alpha=1}^2 \frac{2 - 2\cos(k_\alpha \Delta x_\alpha)}{(\Delta x_\alpha)^2} \Delta t \delta_{ij} . \quad (23)$$

Obviously, in Eq.(23) the last term is required to improve the numerical stability. How to chose the  $\lambda_i$  is the key problem here. It will not be effective if too small and will result in too additional errors if too large. To get some indication we look back to the last terms in Eqs.(17) and (18) which are regarded as artificial viscosities to reduce the numerical wall-heating phenomena. To simplify the discussion, we choose always  $\Delta x = \Delta y$ . Indicative analysis and numerical tests show that we can choose  $\lambda_i$  around the following way,

$$\lambda_i = \begin{cases} c_1 \Delta x, & i = 0 \\ c_1 \Delta x / 10, & i = 1, 2, 3, 4 \\ 0, & i = 5, 6, 7, 8 \end{cases} . \quad (24)$$

Now we show some results of von Neumann analysis by Mathematica-5 to get a more complete understanding of the stability condition. We will show only the results for high-Mach-number flows where the instability problem is generally much more pronounced and previous LB models fail to work. The results will be shown by figures with curves for the maximum eigenvalue  $|\omega|_{max}$  of  $\mathbf{G}$  versus  $k\Delta x$ . The wave number  $k$  is discretized from 0 to  $\pi$  with 30 steps. Figure 2 shows a comparison between the two cases, with and without the additional dissipation term, where the macroscopic variables are chosen as  $\rho = 1.0, T = 1.0, u_1 = 10.0, u_2 = 0.0$ , and the constants in Eqs.(9) and (10) are set as  $c_1 = 10, c_2 = 20, \eta_0 = 10$ . Coefficient  $\alpha$  in the inset of the figure is a new constant introduced to control the time step in the following way,  $\Delta t = \alpha \Delta x / c_2$ . For the two sets of results shown in the figure, it is clear that the dissipation term can significantly decrease the the maximum eigenvalue  $|\omega|_{max}$  from being larger than to be smaller than 1 for appropriately given time step.

It is interesting to investigate the effects of various parameters (physical quantities and model constants in Eqs.(9) and (10)) on the numerical stability. Fig.3 shows the a comparison of two cases: the first one is  $\beta = 0.25$  with switching on the additional dissipation and the second is  $\beta = 0$  with switching off of the additional

8 Pan, Xu, Zhang, Jiang

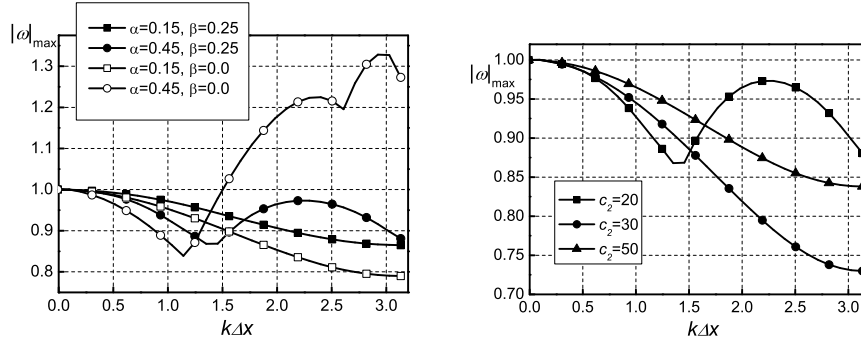


Fig. 3. (Left above) Stability analysis for mixed schemes. The macroscopic variables are set as  $\rho = 1.0, T = 1.0, u_1 = 10.0, u_2 = 0.0$ , the constants are set as  $c_1 = 10, c_2 = 20, \eta_0 = 10, \Delta t = \alpha \Delta x / c_2$ .

Fig. 4. (Right above) The influence of  $c_2$ . The macroscopic variables are set as  $\rho = 1.0, T = 1.0, u_1 = 10.0, u_2 = 0.0$ , the other constants are set as  $c_1 = 10, \eta_0 = 10, \Delta t = 0.45 \Delta x / c_2$ .

dissipation. The latter corresponds to the conventional first-order upwind scheme. For the given parameters, when the time step is small, both treatments give stable simulations; but when the time step becomes large, the first treatment makes the simulation stable while the second one does not.

Figure 4 shows an investigation to the influence of constant  $c_2$  on the stability of LB simulation, where the value of  $c_2$  is altered from 10 to 50, the time step  $\Delta t = 0.45 \Delta x / c_2$ , the other constants and macroscopic variables are unchanged. The LB is stable for all tested values of  $c_2$ . Our experience shows that the value of  $c_2$  does not influence much the numerical stability if it is not smaller than  $2c_1$ , but the stable time step becomes smaller for larger the value of  $c_2$ . Figure 5 shows an investigation to the influence of the value of  $\eta_0$ . The value of  $\eta_0$  is altered from 5 to 20,  $c_2 = 20, \Delta t = 0.3 \Delta x / c_2$ , the other constants and macroscopic variables are kept unchanged. We get an indication that it is not difficult to find an appropriate value of  $\eta_0$  to get a stable simulation. For cases shown in the figure, only a too small value of  $\eta_0$  may result in instability (see the case of  $\eta_0 = 5$ ) and stability is nearly the same when  $\eta_0$  exceeds some critical value (see the cases with  $\eta_0 = 15$  and with  $\eta_0 = 20$ ).

Since the density  $\rho$  can be normalized to 1, we then investigate only the effects of the other two physical quantities, temperature  $T$  and flow velocity  $\mathbf{u}$ . Figure 6 shows three cases with different temperatures,  $T = 1, T = 5$  and  $T = 25$ . When other parameters are fixed, the numerical stability increase with the increasing of the system temperature. This can also be understood that higher temperature corresponds to higher sound speed and lower Mach number.

Figure 7 shows cases with difference flow velocities. The value of  $u_1$  is altered from zero to 15 and  $u_2 = 0$ . For parameters used in this case, we can find that the



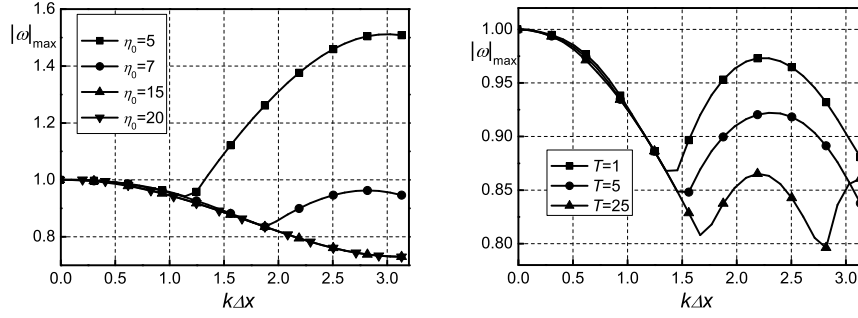


Fig. 5. (Left above) The influence of  $\eta_0$ . The three physical quantities are set as  $\rho = 1.0, T = 1.0, u_1 = 10.0, u_2 = 0.0$ , and other constants are set as  $c_1 = 10, c_2 = 20, \eta_0 = 10, \Delta t = 0.3\Delta x/c_2$ .

Fig. 6. (Right above) The influence of temperature  $T$ . The other physical quantities are set as  $\rho = 1.0, u_1 = 10.0, u_2 = 0.0$ , the constants are set as  $c_1 = 10, c_2 = 20, \eta_0 = 10, \Delta t = 0.45\Delta x/c_2$ .

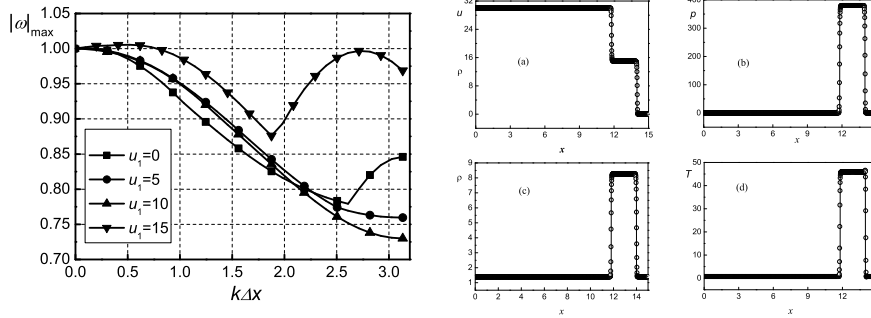


Fig. 7. (Left above) The influence of flow velocity  $u_1$ . The other physical quantities are set as  $\rho = 1.0, T = 1.0, u_2 = 0.0$ , the constants are set as  $c_1 = 10, c_2 = 20, \eta_0 = 10, \Delta t = 0.3\Delta x/c_2$ .

Fig. 8. (Right above) The  $x$  dependence of  $\rho, p, u$  and  $T$ . The symbols are simulation results by the new LB and lines are analytic solutions. The initial condition is described by Eq. (25). Here  $\Delta x = 0.01, \Delta t = 0.00008, c_1 = 25, c_2 = 50, \eta_0 = 30$ , terminal time  $t = 0.36$ .

simulation will not be stable if  $u_1$  is much larger than  $c_1$ , even though  $|\omega|_{\max}$  is only slightly larger than 1 at  $k\Delta x \approx 0.5$ . Our experience shows that the value of  $c_1$  can be set nearly equal to the maximum of the flow velocity.

In summary, constants  $c_1, c_2$  and  $\eta_0$  influence heavily the stability. In practical simulations,  $c_1$  can be set approximately equal to the maximum of flow velocity;  $c_2$  can be set to be about  $2 \sim 3$  times of the value of  $c_1$ ;  $\eta_0$  can be set an appropriate value in between  $c_1$  and  $c_2$ . Equation (24) is indicative in choosing parameters for stable LB simulations of high-speed flow.

10 *Pan, Xu, Zhang, Jiang*

#### 4. Numerical validations

Two kinds of benchmarks are used to validate the proposed scheme. The first one is the Riemann problem. The second is the problem of shock reflection.

##### 4.1. Riemann problem

Here the two-dimensional model is used to solve the one-dimensional Riemann problem. The initial macroscopic variables at the two sides are  $\rho_L$ ,  $p_L$  and  $u_L$ , and  $\rho_R$ ,  $p_R$  and  $u_R$ , respectively. We firstly simulate a Riemann problem with an initial condition described by

$$\begin{aligned}\rho_L &= 1.4, & \rho_R &= 1.4, \\ p_L &= 1.0, & p_R &= 1.0, \\ u_L &= 30.0, & u_R &= 0.0,\end{aligned}\tag{25}$$

where the subscripts “L” and “R” denote the left and right sides of the discontinuity. The initial Mach number of left flow is equal to 30.0. The numerical results for  $\gamma = 1.4$  are shown in Fig.8, where the symbols are simulation results and solid lines are analytical solutions. The parameters used in the simulation are  $c_1 = 25$ ,  $c_2 = 50$ ,  $\eta_0 = 30$ ,  $t = 0.36$ . The size of grid is  $\Delta x = \Delta y = 0.01$ . Time step  $\Delta t = 0.00008$ . The two sets of results have satisfying agreement. In this case no evident “wall-heating” phenomenon is observed. As a comparison, we show a result with the general first order upwind scheme for the pressure in Fig.9(a). A abrupt decrease in pressure around  $x = 12$  corresponds to the well known wall-heating phenomenon. In order to observe the effects of various additional viscosity, we vary the value of  $\lambda_0$  from  $c_1\Delta x$  to  $5c_1\Delta x$  under the fixed  $\lambda_i (i = 1, \dots, 8)$ . Figure 9 (b) shows the simulation results and the exact one. We can find that the numerical width of shock becomes wider and wall-heating problem becomes more pronounced as  $\lambda_0$  increases. Results in Fig. 9 confirm that (24) is indicative in choosing the additional viscosity.

The second example is the propagation of a shock with high ratios of density and pressure. The initial macroscopic variables are give by

$$\begin{aligned}\rho_L &= 1000.0, & \rho_R &= 1.0, \\ p_L &= 1000.0, & p_R &= 1.0, \\ u_L &= 0.0, & u_R &= 0.0,\end{aligned}\tag{26}$$

The size of grid is  $\Delta x = \Delta y = 2.5 \times 10^{-3}$ . The numerical results are shown for  $\gamma = 1.4$  in Fig.10, where the symbols are simulation results and solid lines correspond to exact solutions. We find also a good agreement between the two sets of results.

##### 4.2. Shock reflection

We will present two gas dynamics simulations. Both are done on rectangular grid. The first is to recover a steady regular shock reflection. The second test problem is the double Mach reflection of a shock off an oblique surface. This example is used

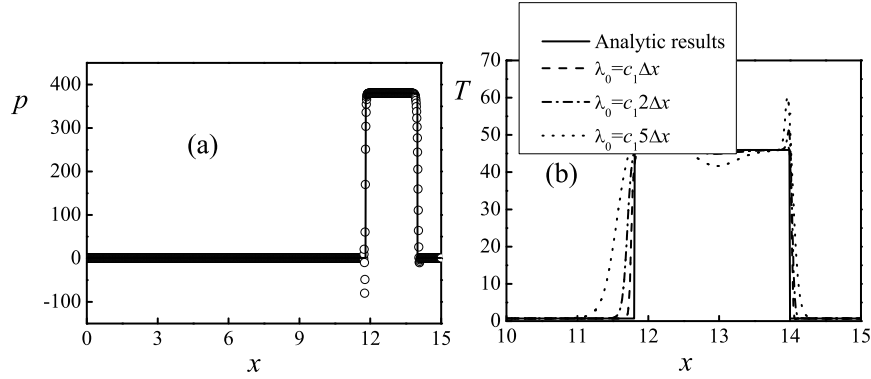


Fig. 9. Comparison of various finite-difference schemes (a) and artificial viscosities (b). The initial condition is same as Fig.8. Here  $\Delta x = 0.01$ ,  $\Delta t = 0.00008$ ,  $c_1 = 25, c_2 = 50, \eta_0 = 30$ ,  $t = 0.36$ . (a) Profile of pressure. The values of  $\lambda_i (i = 0, \dots, 8)$  are the same as those in Fig.8, while  $\beta = 0$ . The symbols correspond to simulation result the line is for analytic solution. (b) Profile of temperature. The dashed, dash dotted and dotted lines correspond to  $\lambda_0 = c_1 \Delta x$ ,  $2c_1 \Delta x$ , and  $5c_1 \Delta x$ , respectively. The values of  $\lambda_i (i = 1, \dots, 8)$  and  $\beta$  are the same as in Fig.8.

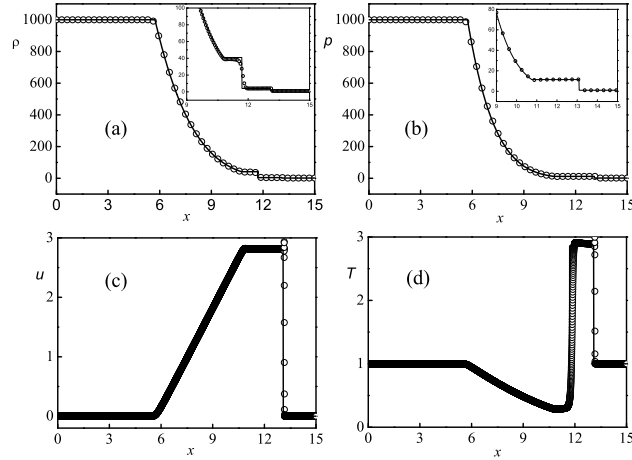


Fig. 10. The  $x$  dependence of  $\rho$ ,  $p$ ,  $u$  and  $T$ . The symbols are simulation results by the new LB and lines are analytic solutions. The initial condition is described by Eq. (26). The used parameters are  $\Delta x = 0.0025$ ,  $\Delta t = 0.0002$ ,  $c_1 = 3, c_2 = 9, \eta_0 = 5$ , terminal time  $t = 1.5$ .

in Ref. <sup>30</sup> as a benchmark test for comparing the performance of various difference methods on problem involving strong shocks.

In the first test problem, we have performed a  $30^\circ$  shock reflection for  $\gamma = 1.4$ . The computational domain is a rectangle with length 9 and height 3 (See Fig.11(a)).

12 *Pan, Xu, Zhang, Jiang*

Fig. 11. (See Fig11.jpg )(Color online) Regular shock reflection. (a), Sketch map of the steady state regular reflection problem. (b), The density contour at time  $t = 2.5$  with  $\Delta x = \Delta y = 0.01$ ,  $\Delta t = 1.5 \times 10^{-4}$ ,  $c_1 = 10, c_2 = 20, \eta_0 = 15$ ; Left and up boundary conditions are given by Eq.(27). From black to yellow, the value increases.

Fig. 12. (See Fig12.jpg )(Color online) Double Mach reflection. (a) initial configuration; (b) the density contour at time  $t = 1.5$  with  $\Delta x = \Delta y = 0.01$ ,  $\Delta t = 2.0 \times 10^{-4}$ ,  $c_1 = 8, c_2 = 16, \eta_0 = 10$ . The reflecting wall begins at 20 mesh length from the lower left corner. From black to yellow, the value increases.

This domain is divided into a  $900 \times 300$  rectangular grid with  $\Delta x = \Delta y = 0.01$ . The boundary conditions are composed of a reflecting surface along the bottom boundary, supersonic outflow along the right boundary, and Dirichlet conditions on the other two sides, given by

$$\begin{aligned} (\rho, u_1, u_2, p)|_{0,y,t} &= (1.0, 10.0, 0.0, 1/1.4) \\ (\rho, u_1, u_2, p)|_{x,1,t} &= (5.0, 8.0, -3.4641, 20.7143) \end{aligned} \quad (27)$$

Initially, we set the solution in the entire domain to be that at the left boundary, the corresponding Mach number is 10.0. In Fig.11(b) we show a contour plot of the density. The clear shock reflection on the wall agrees well with the exact solution.

The second test problem is an unsteady shock reflection. A planar shock is incident on an oblique surface with the surface at a  $30^\circ$  angle to the direction of propagation of the shock (Fig.12(a)). The fluid in front of the shock has zero velocity, and the shock Mach number is 10.0. In Fig.12(b) we show the result of density contour, where the double Mach reflection phenomenon is successfully recovered.

## 5. Conclusions and discussions

The lattice Boltzmann simulation to high-speed compressible flows is revisited by proposing an improved LB model. The new LB model is composed of the original discrete-velocity-model by Kataoka and Tsutahara and an appropriate finite-difference scheme to the convection term. An additional dissipation term is introduced to improve the numerical stability. The adding of the dissipation term should survive the dilemma of stability versus accuracy. In other words, the dissipation should be minimal but make the evolution satisfy the von Neumann stability condition. The effects of polynomial equilibria<sup>19</sup> are taken into account (via the first term of Eq.(23)) in such an approach. Due to the complexity the analysis resorts to the software, Mathematica-5, and only some typical results are shown by figures.

Benchmark tests are used to validate the proposed scheme and reference values of model parameters are suggested. Typical Riemann problems with high-Mach-number (30 or higher) and high ratios (1000 : 1) of pressure and density show good accuracy and stability of the new scheme, even though they are generally difficult to resolve by traditional computational fluid dynamics. Regular and Mach shock reflection problems are successfully recovered, which shows also the potential application of lattice Boltzmann model to fluid systems where non-equilibrium processes

are intrinsic and pronounced. The new LB model may be used to investigate some long-standing problem, such as the transition between regular and shock reflections. At the moment, we are still not able to present a complete description on the most appropriate additional dissipation term, but the idea presented in the paper can be easily used to get some practically useful solutions for stability enhancement. We plan to better clarify the physical dissipation and artificial ones in the future.

### acknowledgments

We warmly thank Profs. Jianshi Zhu, Xingping Liu, Xijun Yu, Zhijun Shen, and Yingjun Li for helpful discussions. Suggestions from the anonymous referee are gratefully acknowledged. This work is partly supported by the National Basic Research Program [Grant No. 2005CB321700], National Natural Science Foundation [Grant No. 10474137] of China, and Science Foundation of Laboratory of Computational Physics, Institute of Applied Physics and Computational Mathematics, Beijing, China.

### References

1. H. S. Shui, *Discrete Methods for One-dimensional Hydrodynamics* (in Chinese), National Defence Industry Press, Beijing (1998).
2. K. Xu, *Gas-kinetic Schemes for Unsteady Compressible Flow Simulations*, von Karman Institute for Fluid Dynamics Lecture Series 1998-03; K. Xu and J. Hu, *J. Comput. Phys.* **142**, 412 (1998).
3. Xijun Yu and Qingfang, *Numer. Methods for Part. Diff. Equat.* **22**, 1455 (2006); Qingfang Dai and Xijun Yu, *SIAM J. Sci. Comput.* **28**, 805 (2006).
4. R. Benzi, S. Succi, and M. Vergassola, *Phys. Rep.* **222**, 145 (1992); D. A. Wolf-Gladrow, *Lattice gas cellular automata and lattice Boltzmann models*, Springer-Verlag, New York (2000); S. Succi, *The lattice Boltzmann equation for Fluid Dynamics and Beyond*, Oxford University Press, New York (2001); H. Chen, S. Kandasamy, S. Orszag, R. Shock, S. Succi, and V. Yakhot, *Science* 301, 633 (2003).
5. J. Horbach and S. Succi, *Phys. Rev. Lett.* **96**, 224503 (2006).
6. E. Orlandini, M. R. Swift, and J. M. Yeomans, *Europhys. Lett.* **32**, 463 (1995); M. R. Swift, E. Orlandini, W. R. Osborn, and J. M. Yeomans, *Phys. Rev. E* **54**, 5041 (1996); G. Gonnella, E. Orlandini, and J. M. Yeomans, *Phys. Rev. Lett.* **78**, 1695 (1997); *Phys. Rev. E* **58**, 480 (1998).
7. Aiguo Xu, G. Gonnella, and A. Lamura, *Phys. Rev. E* **74** 011505(2006); *Phys. Rev. E* **67**, 056105 (2003); *Physica A* **331**, 10 (2004); *Physica A* **344**, 750 (2004); *Physica A* **362**, 42 (2006); Aiguo Xu, *Commun. Theor. Phys.* **39**, 729 (2003).
8. Aiguo Xu, G. Gonnella, A. Lamura, G. Amati, and F. Massaioli, *Europhys. Lett.* **71**, 651 (2005).
9. Aiguo Xu, S. Succi, B. M. Boghosian, *Math. Comput. Simulat.* **72**, 249 (2006).
10. S. Ansumali, I. V. Karlin, *Phys. Rev. Lett.* **95**, 260605 (2005); S. S. Chikatamarla, S. Ansumali, and I. V. Karlin, *Phys. Rev. Lett.* **97**, 010201 (2006).
11. T. Seta and R. Takahashi, *J. Stat. Phys.* **107**, 557 (2002).
12. Z. Guo and T. S. Zhao, *Phys. Rev. E* **67**, 066709 (2003).
13. M. Watari and M. Tsutahara, *Phys. Rev. E* **67**, 036306 (2003); *Phys. Rev. E* **70**, 016703 (2004).

14 *Pan, Xu, Zhang, Jiang*

14. T. Kataoka and M. Tsutahara, Phys. Rev. E **69**, 035701(R) (2004).
15. T. Kataoka and M. Tsutahara, Phys. Rev. E **69**, 056702 (2004).
16. H. Chen, Phys. Rev. E **58**, 3955(1998); H. Xi, G. Peng, and S. H. Chou, Phys. Rev. E **60**, 3380 (1999); S. Ubertini, G. Bella, and S. Succi, Phys. Rev. E **68**, 016701 (2003).
17. Y. Li, Eugene J. LeBoeuf, and P. K. Basu, Phys. Rev. E **69**, 065701(R) (2004); *ibid.* **72**, 046711 (2005).
18. F. J. Alexander, H. Chen, S. Chen, and G.D.Doolen, Phys. Rev. A **46**, 1967 (1992); Y.H.Qian and S. A. Orszag, Europhys. Lett. **21**, 255 (1993); G. Yan, Y. Chen and S. Hu, Phys. Rev. E **59**, 454 (1999); Y. Chen, H. Ohashi and M. Akiyama, Phys. Rev. E **50**, 2776 (1994); C. Sun, Phys. Rev. E **58**, 7283 (1998); *ibid.* **61**, 2645 (2000); Aiguo Xu, Europhys. Lett. **69**, 214(2005); Aiguo Xu, Phys. Rev. E **71**, 066706 (2005).
19. W. A. Yong and L. S. Luo, Phys. Rev. E. **67**, 1063(2003).
20. P. Bhatnagar, E. P. Gross, and M. K. Krook, Phys. Rev. **94**, 511 (1954).
21. A. Xiong, Acta Mech. Sinica (English Series) **18**, 603 (2002).
22. G. J. Ball, Shock Waves, **5**, 311(1996).
23. F. Tosi, S. Ubertini, S. Succi, H. Chen, I.V. Karlin, Math. Comput. Simulat. **72**, 227(2006)
24. S. Ansumali, I. V. Karlin, J. Stat. Phys. **107**, 291(2002); S. Ansumali, I. V. Karlin, H. C. Ottinger, Europhys. Lett. **63**, 798(2003)
25. Y. Li, R. Shock, R. Zhang, H. Chen, J. Fluid Mech. **519**, 273(2004)
26. V. Sofonea, A. Lamura, G. Gonnella, A. Cristea, Phys. Rev. E **70** 046702 (2004).
27. R. A. Brownlee, A. N. Gorban and J. Levesley, Phys. Rev. E. **75**, 036711 (2007)
28. J. D. Sterling and S. Chen, J. Comput. Phys. **123**, 196 (199).
29. X. D. Niu, C. Shu, Y. T. Chew, and T. G. Wang, J. Stat. Phys. **117**, 665 (2004).
30. P. R. Woodward and P. Colella, J. Comput. Phys. **54**, 115(1984).

This figure "Fig11.jpg" is available in "jpg" format from:

<http://arxiv.org/ps/0706.0405v1>

This figure "Fig12.jpg" is available in "jpg" format from:

<http://arxiv.org/ps/0706.0405v1>